ADVANCED FUNCTIONAL MATERIALS
www.afm-journal.de

Decoupling Nucleation and Growth in Fast Crystallization of Phase Change Materials

*Maximilian J. Müller, Carmen Morell, Peter Kerres, Mohit Raghuwanshi, Ramon Pfeiffer, Sebastian Meyer, Christian Stenz, Jiangjing Wang, Dmitry N. Chigrin, Pierre Lucas, and Matthias Wuttig**

Disentangling nucleation and growth in materials that crystallize on the nanosecond time scale is experimentally quite challenging since the relevant processes also take place on very small, i.e., sub-micrometer length scales. Phase change materials are bad glass formers, which often crystallize rapidly. Here systematic changes in crystallization kinetics are shown in pseudo-binary compounds of GeTe and Sb_2Te_3 and related solids subjected to short laser pulses. Upon systematic changes in stoichiometry, the speed of crystallization changes by three orders of magnitude concomitantly with pronounced changes in stochasticity. Resolving individual grains with electron backscatter diffraction (EBSD) permits to disentangle of the process of nucleation and growth. From these experiments, supported by multiphysics simulations of crystallization, it can be concluded that high crystallization speeds with small stochasticity characterize phase change materials with fast nucleation, while compounds that nucleate slowly crystallize much more stochastically.

1. Introduction

The crystallization of glasses or amorphous solids is a key component of many technological developments ranging from zero thermal expansion ceramics[1] to non-volatile memories.[2–4] It also remains a source of controversy in the study of systems as fundamental as water.[5,6] Our understanding of crystallization has been greatly improved by studying glass formers with sluggish kinetics to resolve the relative contribution of nucleation and growth during crystallization.[7] In systems such as lithium disilicate, traditional experimental methods like optical or electron microscopy enable the distinct determination of nucleation and growth rates. In contrast, resolving the nucleation and growth of poor glass formers such as phase change materials (PCMs) is significantly more difficult due to extremely fast kinetics and the small length scale of nucleation. Yet, controlling nucleation and growth in the fast regime is essential to the development of the next generations of PCM technologies such as neuromorphic computing or multi-level high-density memories.[8] The development of such devices rests on the ability to controllably and rapidly induce partial crystallization of a PCM cell through a sequence of electrical or optical pulses to encode multi-level information in the form of resistivity or reflectivity steps.[8] Furthermore, upon priming, the switching speed can be increased by orders of magnitude upon controlling the formation of subcritical nuclei.[9] In either case, characterizing and

M. J. Müller, C. Morell, M. Raghuwanshi, R. Pfeiffer, S. Meyer, C. Stenz, J. Wang, D. N. Chigrin, M. Wuttig
Institute of Physics
Physics of Novel Materials
RWTH Aachen University
52056 Aachen, Germany
E-mail: wuttig@physik.rwth-aachen.de

P. Kerres, M. Wuttig
PGI 10 (Green IT)
Forschungszentrum Jülich GmbH
52428 Jülich, Germany

The ORCID identification number(s) for the author(s) of this article can be found under https://doi.org/10.1002/adfm.202403476

DOI: 10.1002/adfm.202403476

M. Raghuwanshi
Fraunhofer Institute for Applied Solid State Physics IAF
79108 Freiburg, Germany

J. Wang
Center for Alloy Innovation and Design (CAID)
State Key Laboratory for Mechanical Behavior of Materials
Xi'an Jiaotong University
Xi'an 710049, China

D. N. Chigrin
DWI-Leibniz-Institut für Interaktive Materialien
Forckenbeckstrasse 50, 52074 Aachen, Germany

P. Lucas
Department of Materials Science and Engineering
University of Arizona
Tucson, AZ 85721, USA

M. Wuttig
Jülich-Aachen Research Alliance (JARA FIT and JARA HPC)
RWTH Aachen University
52056 Aachen, Germany

understanding the decoupling between nucleation and growth is critical to select a PCM featuring the appropriate crystallization characteristics. In addition to speed, the stochasticity of the process also plays a crucial role. For example, a highly stochastic crystallization can affect the efficiency and precise controllability of applications. On the other hand, a stochastic switching process can be used to solve computational problems efficiently, i.e., close to hardware, such as the generation of true random numbers.[10] Since crystallization parameters are critical to any PCM device, they have been studied using a broad range of techniques including calorimetric,[2,11] optical[3], and electrical measurements.[8,9,12,13] Yet, so far none of these approaches has enabled the decoupling of nucleation and growth at the high rates relevant to technological applications, by means of experiments that also provide high spatial resolution to characterize the crystallization mechanism. Here, we combine fast reflectance measurements and electron backscatter diffraction (EBSD) to decouple nucleation and growth in five PCMs which differ in crystallization speed by more than 3 orders of magnitude. These differences are shown to be caused by differences in nucleation rate, while the crystal growth rate is nearly independent of stoichiometry. This finding also explains why the fast-nucleation materials crystallize significantly less stochastically than the slow-nucleation materials, a difference that is crucial for device applications.

Crystallization is a phase transition driven by the difference in Gibbs free energy between the crystalline phase and the undercooled liquid.[14] Right at the melting temperature, this difference is zero. Hence, there is no driving force for crystallization. Cooling the material below the melting temperature creates a driving force for crystallization ($\Delta G < 0$). However, an activation barrier needs to be overcome until a crystalline precursor – a nucleus – is created in the undercooled liquid. The formation of such a nucleus can be described by the classical nucleation theory. To meet the thermodynamic condition for a nucleus to grow the Gibbs free energy gained minus the interfacial energy has to be at its maximum or beyond it. This way growth of a crystalline nucleus is more likely than its shrinkage. This only happens above a certain critical nucleus size. This critical nucleus size decreases with decreasing temperature, since the interfacial energy is approximately independent of temperature,[15] while the Gibbs free energy difference increases with decreasing temperature. The formation of critical nuclei is a stochastic process that depends on the size distribution of subcritical nuclei, i.e., nuclei that are slightly smaller than the critical nucleus. Due to the growth and shrinkage of clusters, the initial size distribution changes with time. This phase is called transient nucleation.[16] After some time, the distribution enters a so-called steady state in which the nuclei continue to grow and shrink because they are not thermodynamically stable. Yet, the overall distribution remains constant due to the time-independent transition rates between different nuclei sizes. This steady-state nucleation was derived by Volmer and Weber in 1926[17] and has been used and refined continuously thereafter in a variety of theoretical[18,19] and experimental[20,21] studies.

Density functional theory (DFT) is usually unable to characterize the formation of (sub-)critical nuclei.[9,22] This process is generally too slow and involves a critical nucleus size that exceeds the typical length scale of several hundred to thousands of atoms that can be handled by DFT with ease. Yet, critical nuclei as small as 2–3 nm have been reported for PCMs.[23] Very recently even system sizes of $40 \times 20 \times 20$ nm^3 have been handled.[24] Furthermore, crystallization has been accomplished in a few nanoseconds and even less. This time and length scale is still challenging but can be addressed by DFT. This explains why this approach has already been used several times to unravel the contribution of nucleation and growth to crystallization in PCMs.[4,25–28] Experimentally, the situation is quite different. Determining the size distribution of the subcritical clusters experimentally is a nontrivial problem, due to the nuclei's very small size. Furthermore, the high speed of the nucleation process in PCMs at elevated temperatures provides a major challenge for experimental investigations. It is quite difficult to homogeneously heat a sample instantaneously to a desired temperature. Frequently, short, and sharply defined, tunable pulses are employed, either as laser or voltage pulses. The pulse length is often identified as the (maximum) time the sample had to crystallize. The extent of crystallization reached after this time can then be measured subsequently (post-mortem), i.e., without time resolution. Measuring for example the change of reflectance upon applying a short laser pulse can help to determine the macroscopic degree of crystallization.

The pronounced property contrast between the crystalline and the glassy state in PCMs facilitates the distinction of both phases. It stems from the different chemical bonding types present in the amorphous and crystalline state. This is a highly unusual situation since it is commonly assumed and recently proven that bonding in the glassy and crystalline state of, e.g., ordinary oxide glasses is the same.[29] For phase change materials, on the contrary, the amorphous state features covalent bonding, while the crystalline state exhibits metavalent bonding.[30,31] Since this is both highly unusual and important to understand phase change materials, we will briefly summarize which knowledge has recently been developed for a large fraction of phase change materials, including the materials discussed here. The crystalline state is characterized by a unique property portfolio[32,33] (a high optical dielectric constant, a large Born effective charge Z^*, a number of nearest neighbors larger than expected for ordinary covalent bonding, anharmonic bonds as seen from a high Grüneisen parameter for transverse optical modes, and a high electrical conductivity at room temperature reaching values of bad metals). Furthermore, metavalent solids are found to have an unconventional bond rupture in laser-assisted field evaporation[34] and are characterized by small charge transfer between the atoms and the sharing of half an electron pair (one electron) between adjacent atoms.[35] These metavalent solids are governed by the interplay between localization and delocalization of electrons.[30] Since the bonding mechanism changes profoundly upon crystallization,[36,37] the material properties also change considerably, facilitating the observation of crystallization in electrical or optical measurements. Consequently, we follow the reflectance changes of the sample as a function of laser pulse length and pulse power. Such data can be fitted by the Johnson-Mehl-Avrami-Kolmogorow-model (JMAK-model)[38] or the phase field model[39] which both rely on reasonable assumptions for the nucleation and growth rate. Hence, to avoid any assumption it would be ideal to determine nucleation and growth rates independently with the required high spatial and temporal resolution.

To decouple these processes, electron backscatter diffraction (EBSD) performed within a scanning electron microscope can be utilized. With EBSD, the size, and orientation of different grains at the surface of a sample can be determined,[40] which is extremely challenging for macroscopic techniques like optical microscopy or x-ray diffraction due to the small size of the examined crystalline grains. Meanwhile, reflectance measurements permit to capture of the kinetics of crystallization even in the fast regime.[3] Earlier EBSD studies like[41] concerning crystallization concentrated on conventional thermally induced crystallization where the corresponding time and length scales of nucleation are considerably larger. In our work, combining precise fast time-resolved optical crystallization experiments with a determination of the resulting grain structure of the crystallized region provides detailed information on the nucleation rate and growth velocity as will be shown for five different phase change materials with pronounced differences in crystallization kinetics. Three compounds were chosen since they are prototypical phase change materials, i.e., GeTe, $Ge_2Sb_2Te_5$, and $Ag_4In_3Sb_{67}Te_{26}$ (AIST). The other two are compounds of GeTe combined with the isoelectronic GeSe and SnTe, i.e., Ge_2SeTe and $Ge_3Sn_2Te_5$, which have been observed to have significantly different crystallization properties compared to GeTe.[42]

2. Power-Time-Effect Diagrams

The crystallization parameters of a given material depend strongly on temperature. Therefore, very fast heat induction into the system is mandatory to enable fast crystallization. This can be achieved in two ways, either electrically by micro heaters[43,44] or optically upon applying well-defined laser pulses.[45] With microheaters, good spatial heat control can be achieved. Nevertheless, elaborate design and testing are needed to utilize such heaters. Additionally, the total induced energy is limited. Pulsed lasers with a well-defined beam profile offer a suitable alternative, providing intense and short heat induction into the system. Therefore, in this study, such laser pulses are used to achieve high temporal resolution. A low-power laser is used to simultaneously perform fast reflectance measurements to quantify the extent of crystallization. The initial samples are fully amorphous sputtered films that contain no nuclei, unlike melt-quenched samples. A selected area electron diffraction (SAED) study of such GeTe samples shows amorphous films without discernible crystalline grains.[46] Further details on the measurements can be found in the supplementary information (Figure S1, Supporting Information). In the current study, the local reflectance change of the sample is measured. The optical properties of the PCM layer are different in the crystalline state compared to the amorphous state, caused by a change in chemical bonding mechanism as well as film density.[30] This leads to a change, usually an increase, in reflectance of the sample. This change is approximately proportional to the crystalline volume fraction in the amorphous phase, as further discussed and simulated in the supplementary information (Figure S4, Supporting Information). By incrementally increasing pulse power as well as pulse length and measuring the reflectance change caused by crystallization a so-called power-time-effect (PTE) diagram is measured. The induced temperature increase is proportional to the laser pulse power. Additionally, the amount of reflectance change locally maps the portion of the sample transformed into the crystalline phase. Therefore, these diagrams can be compared to time-temperature-transformation (TTT) diagrams, which are commonly employed to characterize crystallization. However, there is no one-to-one correspondence, which is further explained in the following. As shown in **Figure 1** the minimum pulse length required to start crystallization differs drastically between materials from 10^2 ns for $Ge_2Sb_2Te_5$ up to 10^5 ns for Ge_2SeTe. Additionally, it can be observed that the faster crystallizing systems, i.e., $Ge_2Sb_2Te_5$ and $Ge_3Sn_2Te_5$ (Figure 1a,b), exhibit a significantly less stochastic crystallization process, compared to the more slowly crystallizing systems GeTe, $Ag_4In_3Sb_{67}Te_{26}$ (AIST) and Ge_2SeTe (Figure 1c–e). Furthermore, it is observed that the onset time of crystallization is approximately independent of power above some threshold power. This leads to a vertical edge in the PTE diagram.[42] Note that the slight increase in reflectance change in the upper left corners of the PTE diagrams can be ascribed to the structural relaxation of the amorphous phase. Furthermore, it is also striking that the minimum power needed to crystallize the sample strongly depends on the sample stoichiometry. This can be explained by the combination of two material properties. The absorption of the laser light mostly depends on the imaginary part of the dielectric function ϵ_2 (and to a lesser extent on film thickness). For the amorphous system of for example the $Ge_2Se_xTe_{1-x}$ pseudo-binary line, it has been shown that ϵ_2 at the pulse-laser wavelength strictly decreases from GeTe to GeSe. This can be attributed to an overall decrease as well as a shift of the maximum of ϵ_2 toward higher energies for GeSe.[37] This explains the high power needed to crystallize Ge_2SeTe. Additionally, the crystallization temperature T_c changes with film stoichiometry. For a constant heating rate of 20 K min^{-1}, a crystallization temperature of 188 °C was measured for GeTe,[47] while $Ge_2Sb_2Te_5$ crystallizes already at 159 °C.[48] Hence, GeTe would require a higher laser power to crystallize an amorphous region. This is in line with the data shown in Figure 1. Similarly, the contrast after crystallization for AIST decreases again above a pulse power of ≈35 mW. This can be attributed to the induced temperature exceeding the optimal temperature for crystallization significantly. The effect is so pronounced for AIST because of its relatively low melting temperature of 817 K,[49] compared to GeTe (1000 K[50]), and $Ge_2Sb_2Te_5$ (889 K[39]), and therefore also lower optimal crystallization temperature.

In order to clarify the origin of the features observed in the PTE plot, a multiphysics simulation has been performed. From such simulations, we expect to obtain answers to the following questions. Why do different materials have different crystallization times? Why does the minimum time to crystallize for a given material hardly depend on the laser pulse power, once a certain threshold is exceeded? This independence is surprising since the different pulse powers should lead to different sample temperatures. In the multiphysics simulation, the optical and thermal properties of the different layer stacks are adequately considered. A transient heat transfer simulation is performed using the experimental sample parameters and laser beam with a radius of 1220 nm. The temperature evolution of the PCM layer is compiled as a function of time and laser power (**Figure 2a**). At this stage, for simplicity of the argument, the influence of the phase transition on the thermal and optical properties of the PCM has been disregarded. We have performed such simulations for

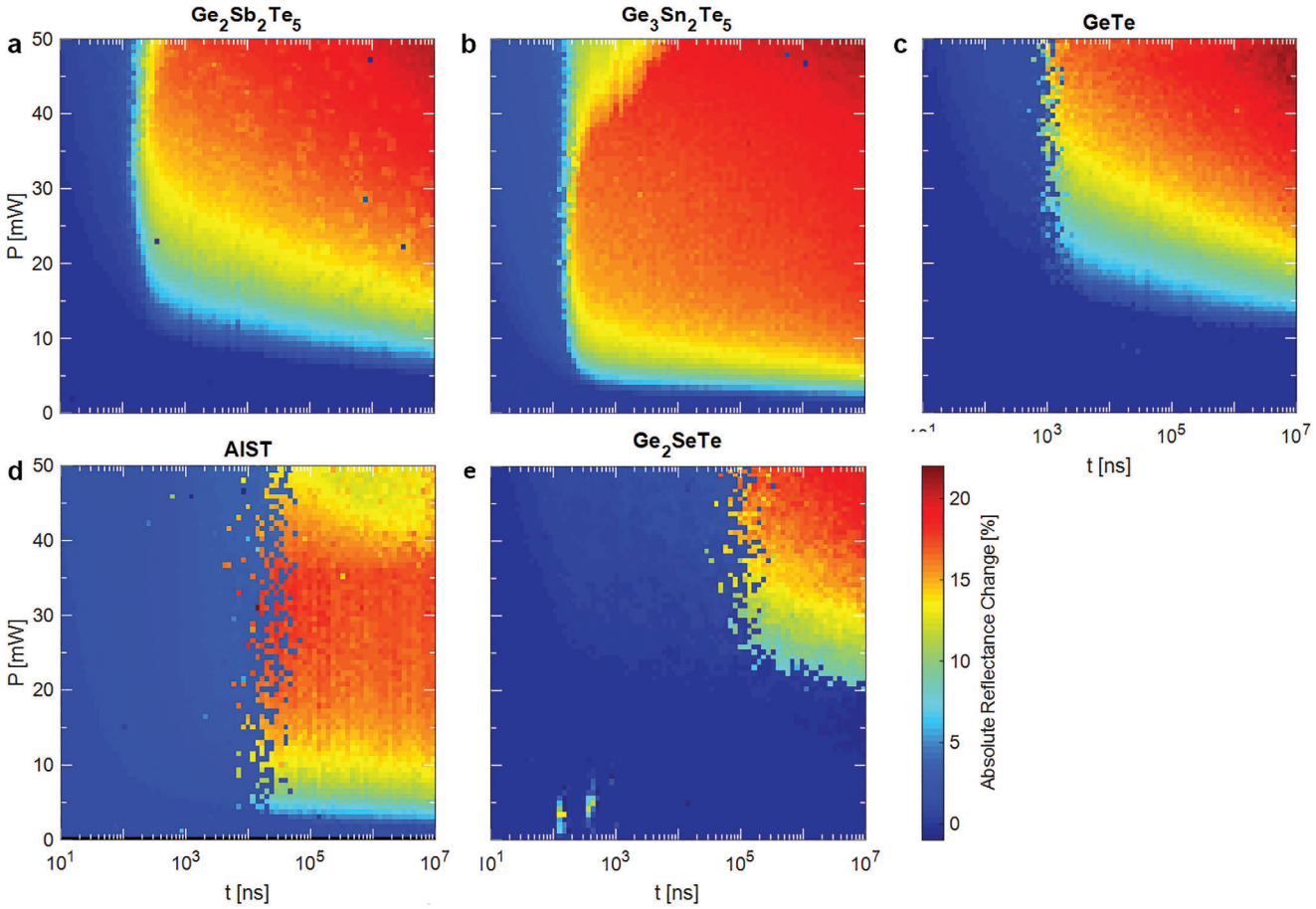

Figure 1. Power-time-effect (PTE) diagrams for five different phase change materials: $Ge_2Sb_2Te_5$ a), $Ge_3Sn_2Te_5$ b), GeTe c), AIST d), and Ge_2SeTe e). Crystallization of the materials leads to a significant increase in reflectance. All materials exhibit a vertical edge, implying that the crystallization speed which results from the nucleation rate and growth velocity is independent of applied power. Significant differences in the minimum time (pulse length) needed to crystallize as well as the stochasticity of this process are observed for the five different materials. The two spots of reflectance change observed for Ge_2SeTe at very low powers and very short pulses can be attributed to local impurities on the sample surface since they are also already observable before the crystallization laser pulse. These impurities seem to be affected already at low pulse powers.

$Ge_2Sb_2Te_5$ and GeTe to better interpret the measured PTE diagrams. As shown in Figure 2a, the temperature in the sample increases in the first 100 ns of a pulse and subsequently reaches a constant steady state temperature which indeed increases linearly with increasing pulse power (Figure 2b. Nevertheless, experimental PTE plots indicate that the minimum time to crystallize hardly depends upon the pulse power, once a critical threshold is exceeded. This striking observation can be attributed to a combination of highly temperature-dependent and only slightly overlapping nucleation rate and growth velocity (as simulated in Figure 2c,d) as well as heating times of 100 ns in the order of the fastest expected isothermal crystallization (Figure 2f). Let us consider two characteristic pulse powers, 25 and 40 mW. For a pulse power of 25 mW, after ≈100 ns, 600 K is reached in the phase change material. At this temperature, the nucleation rate is very high and the growth velocity is still modestly high, too. Thus, fast crystallization can be achieved. At a pulse power of 40 mW, instead, a temperature of 800 K is reached after 100 ns. This temperature is too high for pronounced nucleation but is ideal for fast crystal growth. Yet, at times smaller than 100 ns, the temperature range has already been reached where nucleation is very high. During this time nucleation can occur without significant changes in reflectance, which is often denoted as priming. Since subsequent growth is needed to enable complete crystallization, the exact timing of previous nucleation has a decreased impact on the overall crystallization speed. Hence, for both different pulse powers, a similar crystallization time is obtained. This causes the PTE diagram to develop an almost vertical border of crystallization to start (Figure 2e). In contrast to this, at constant temperature (Figure 2f) fast crystallization is only featured for a small temperature window where fast nucleation and growth overlap. The PTE (TTT) diagram was calculated using the non-isothermal (isothermal) JMAK model. A uniform temperature distribution over the PCM layer was assumed for simplicity. Additionally to this effect, a non-uniformity of the temperature distribution in the illuminated volume also contributes to the development of an almost vertical border of crystallization in the PTE diagram. The temperature gradient away from the center of the laser beam features a fast crystallization temperature for every pulse power above the power needed to induce this temperature in the center

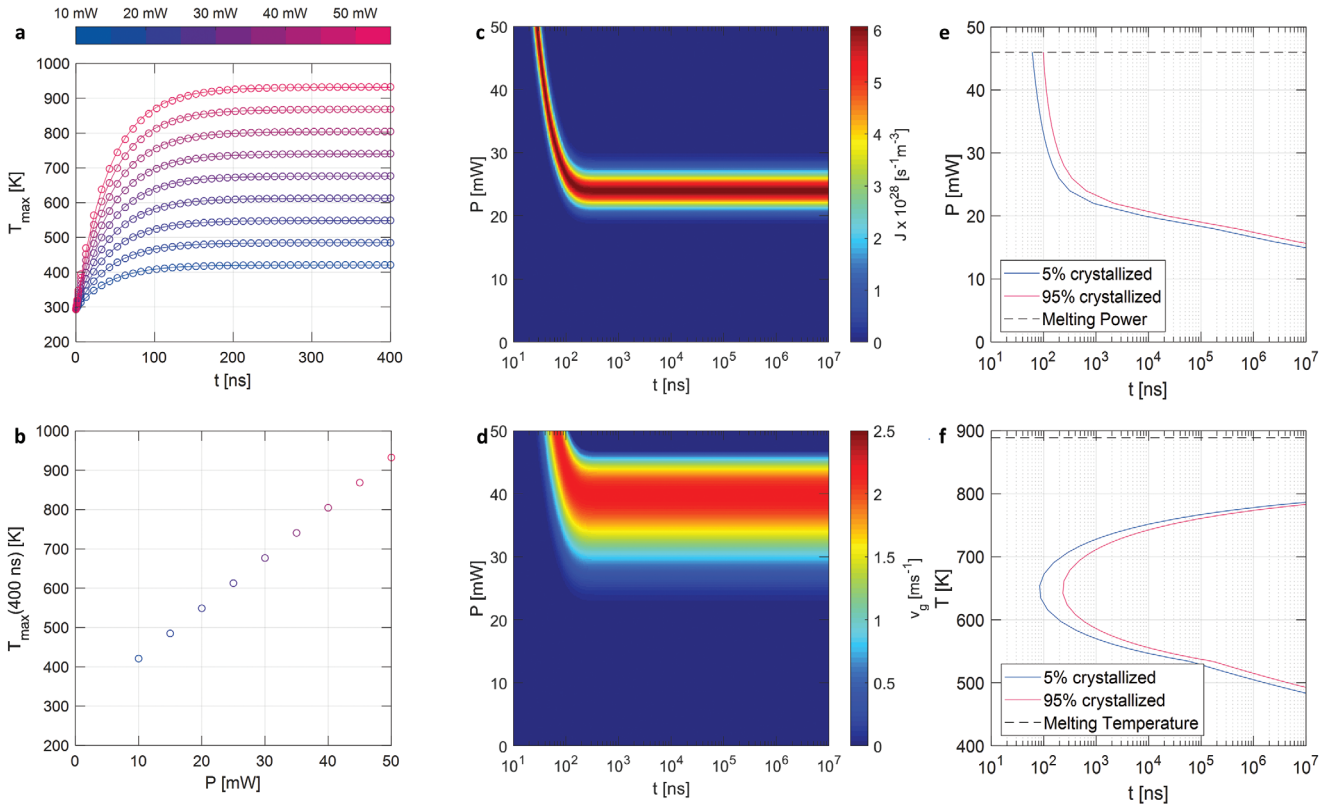

Figure 2. Multiphysics simulation of the crystallization of an amorphous film of $Ge_2Sb_2Te_5$. The maximum temperature in the center of the laser beam increases during the first 100 ns of the pulse a). The final temperatures after 400 ns exhibit a linear dependence on the pulse power b). The steady-state temperature increase depends linearly on the applied laser power. Nucleation rate c) and growth velocity d) change significantly with time for the first ≈100 ns. Further information on how the temperature dependence on nucleation rate and growth velocity were simulated can be found in (Figure S5, Supporting Information). Thus, all pulses above 25 mW reach at some time a temperature range, where rapid nucleation occurs. Thus, the calculated PTE diagram e) exhibits a nearly vertical border, as observed experimentally. In contrast to this, under constant temperature conditions f), fast crystallization is only observed in a narrow temperature window ≈650 K, at which a sweet spot between fast nucleation and fast growth occurs.

of the beam. The temperature of fast nucleation migrates further away from the center for higher power pulses. This results in the coexistence of some regions within the PCM layer (not necessarily overlapping) that have a near-optimal temperature for both nucleation and growth during the laser illumination. A more detailed explanation can be found in the supplementary information (Figure S7, Supporting Information). Both effects decrease the influence of ule power in the crystallization speed and therefore result in the observed vertical edge in the PTE diagram.

Since the crystallization process is not governed by the applied laser power once a threshold is surpassed, we can get better statistics if we just apply pulses of the same power, which are given in Table S1 (Supporting Information) in the supplementary information, and vary the pulse length. The results of such experiments are depicted in **Figure 3**, which shows the evolution of the sample reflectance upon laser excitation for different pulse lengths. This figure reveals an interesting correlation between the crystallization speed and the stochasticity of the process. For materials that crystallize rapidly, there is very little stochastic variation. For each pulse length, the effect on reflectance and therefore crystal volume fraction can be predicted very well. There are only minor deviations from this prediction. A continuous crystallization exhibiting only low stochasticity could be desirable to implement multi-level memory applications including neuromorphic devices.[51] However, for materials that crystallize slowly, the process is much more stochastic. For these systems, the material will be either crystalline (high reflectance) or amorphous (low reflectance) after the pulse. Whether crystallization happens or not can therefore only be described stochastically and not deterministically as for the rapidly crystallizing systems.

3. Electron Backscatter Diffraction Measurements

To unravel the origin of the different crystallization stochasticities, crystalline spots are examined with electron backscatter diffraction (EBSD). To produce crystalline spots for this purpose, pulse powers identical to the measurements depicted in Figure 3 were selected. To obtain a completely crystallized spot the pulse length was chosen as the longest pulse length in Figure 3 for each material, i.e., 1.5×10^3 ns for $Ge_2Sb_2Te_5$ and $Ge_3Sn_2Te_5$, 1.5×10^4 ns for GeTe, 1.5×10^5 ns for AIST and 2×10^6 ns for Ge_2SeTe.

Interestingly, a general correlation between the minimum time required to crystallize and the grain distribution is found. For $Ge_2Sb_2Te_5$ and $Ge_3Sn_2Te_5$, i.e., the fastest crystallizing materials, many crystalline grains with distinct boundaries can be observed in **Figure** 4a,b. Furthermore, these grains have different

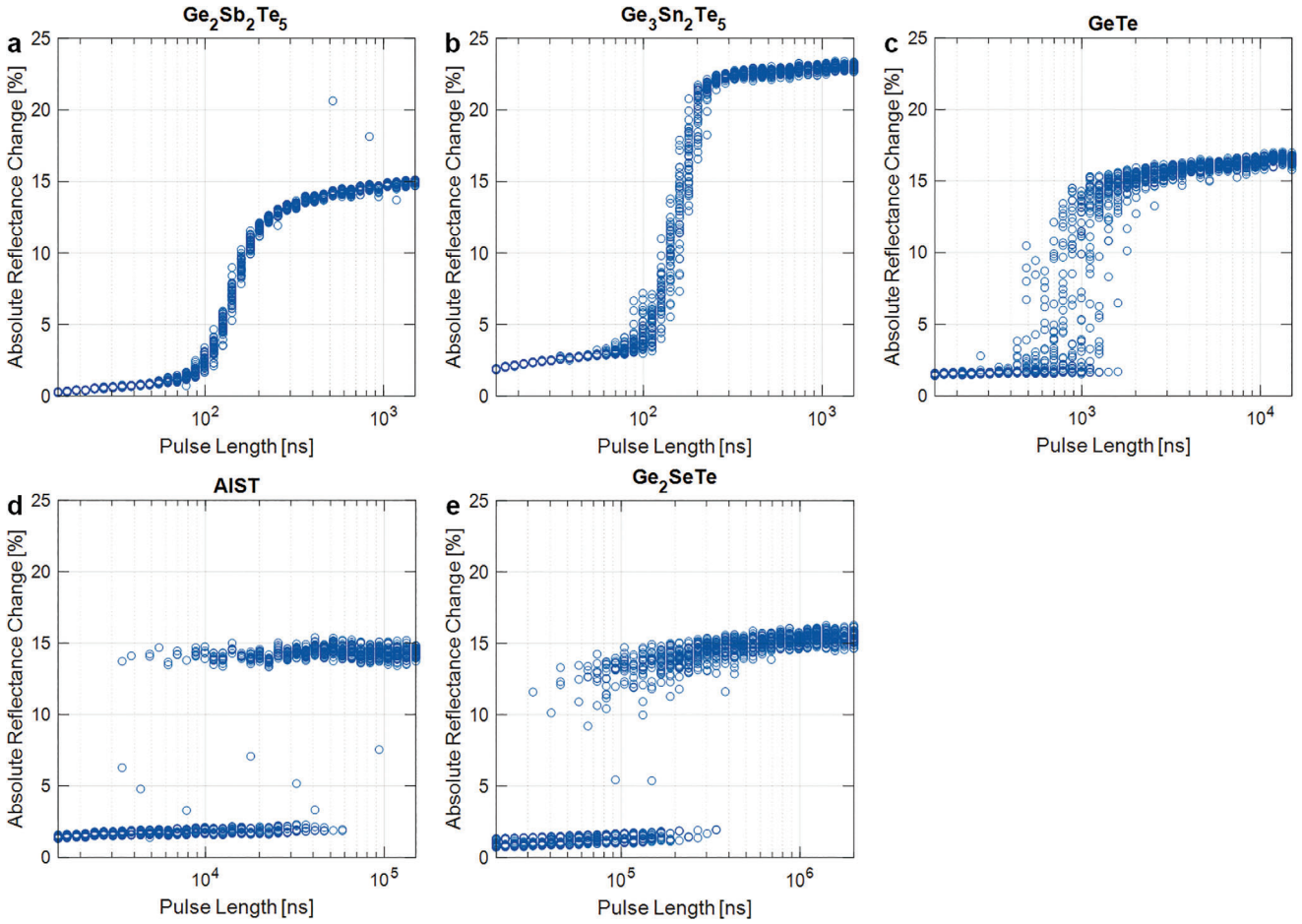

Figure 3. Optically induced crystallization experiments with varying pulse length and constant pulse power. Note that every data point refers to an independent crystallization experiment, rather than a real-time reflectance measurement of a single crystallite. In the case of $Ge_2Sb_2Te_5$ a) and $Ge_3Sn_2Te_5$ b), i.e., the fastest crystallizing materials a continuous transition from the amorphous to the crystalline state can be observed. For GeTe c), Ge_2SeTe d), and AIST e) the transition instead is more stochastic in nature.

sizes and random orientations. This indicates that every grain grew from a separate nucleus. The fact that different grains have different orientations shows that they crystallize independently from each other. The different sizes of the grains are indicative of their "ages", i.e., the corresponding clusters were formed at different times since the growth velocity of the grains should be independent of their orientation in the amorphous matrix. Hence crystalline clusters continue to form even after the first nuclei have crystallized. The sigmoidal shape of the reflectance change observed for $Ge_2Sb_2Te_5$ and $Ge_3Sn_2Te_5$ is a consequence of this interplay of nucleation and growth. This aspect will be discussed in more detail later when we compare our findings with studies performed at lower temperatures and thus smaller crystallization rates.

The EBSD data in Figure 4 and the reflectance change in Figure 3 look very different for the other three phase change materials, i.e., GeTe, AIST, and Ge_2SeTe. This is most clearly seen for Ge_2SeTe, i.e., an equimolar alloy of GeTe and GeSe. In this case, only a single grain orientation is observed, which indicates that the entire grain grew from one nucleus. Apparently, no second nucleus formed in the crystalized region even though a rather long laser pulse of 2×10^6 ns was applied. This already provides evidence for a significantly smaller nucleation rate for Ge_2SeTe, compared to $Ge_2Sb_2Te_5$ and $Ge_3Sn_2Te_5$. The other two EBSD images, i.e., the one for AIST and GeTe look slightly more complex. On the one side, they seem to exhibit changes in grain orientation, as can be seen from the near continuous change of color along the grain. Yet, grains with distinct orientations normally exhibit clear grain boundaries, as observed in Figure 4a,b, instead of a continuous change. In that respect, Kolosov found from detailed TEM investigations of crystallization of phase change materials that these crystallized regions often show "bent planes".[52–54] So-called transrotational crystals[55] arise due to density changes in the border region between amorphous and crystalline material during crystal growth.[56] These "bent" crystals would exhibit a continuous change in apparent orientation even though they correspond to a single grain. Hence, it can be concluded that some materials show fast nucleation ($Ge_2Sb_2Te_5$ and $Ge_2Sn_2Te_5$) where several different nuclei develop in the micron-size region illuminated by the laser pulse, while others show slow nucleation (GeTe, AIST, and Ge_2SeTe), where only a single grain or in the case of GeTe a very low number

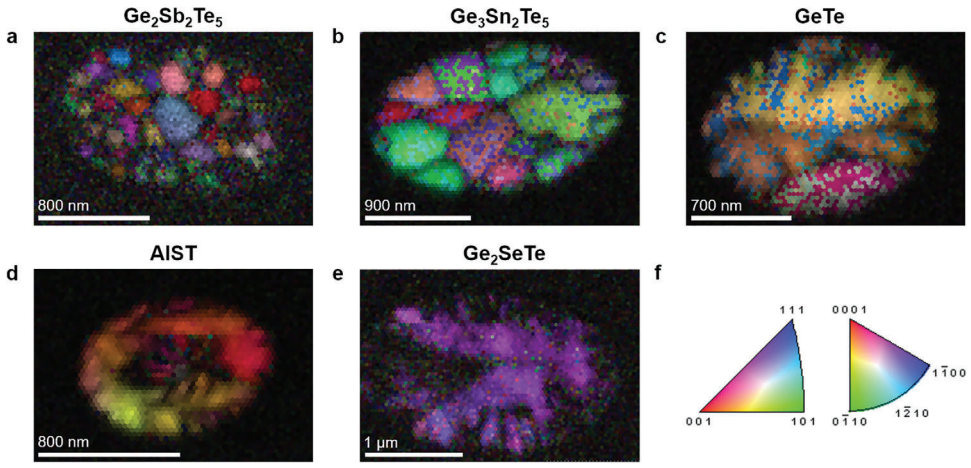

Figure 4. Inverse pole figure (color) and image quality (brightness) of a variety of materials upon crystallization with a laser pulse, measured with electron backscatter diffraction (EBSD). For each material measurements of 5 to 8 individual crystalline spots were taken. Here are prototypical examples of these measurements. In the case of $Ge_2Sb_2Te_5$ a) and $Ge_3Sn_2Te_5$ b) a multitude of grains is observed upon illuminating with short laser pulses, indicative of fast nucleation. For GeTe c) 2 – 3 grains are observed, while for AIST d) and Ge_2SeTe e), only a single grain is observed, as explained in more detail in the text, even though much longer laser pulses are employed than in a) and b). This indicates that nucleation is much slower for these three materials. No crystal grains are observed outside of the main clusters. This reinforces the interpretation of an initially completely amorphous state of the samples. f) Color legends of the inverse pole figure for cubic $Ge_2Sb_2Te_5$ and AIST on the left and for hexagonal $Ge_3Sn_2Te_5$, GeTe, and Ge_2SeTe on the right.

of grains develops in this region. The terms *fast-nucleation* and *slow-nucleation* material have been introduced for phase change materials presumably by Kalb et al.[57] to distinguish these different classes of materials.

The number of grains N_{Grains} per crystalline spot in the EBSD measurements can also be counted. To do so, the number of grains has been averaged from the grains counted in each recorded EBSD image after taking 5 to 8 such images for each material. Further details can be found (Table S2, Supporting Information). AIST was excluded from this analysis since it is hard to count the grains due to the plane bending. From the crystallization data presented in Figure 3, the stochasticity S of the crystallization process can be calculated. This metric is defined as the standard deviation of the reflectance change during crystallization normalized by the reflectance change after crystallization is finished. Detailed information on the calculation can be found (Figure S3, Supporting Information). This metric focuses on the stochasticity of how far the crystallization has advanced after a given pulse. A time-based metric like the distribution of induction times[58] or a method calculating the time variation to reach a given reflectance change differs conceptually since the nucleation time is not measured explicitly here. The time-based metrics concentrate on a specific aspect of crystallization, i.e., nucleation. A further evaluation of the nucleation time will be discussed later. The results are shown in **Figure 5a**, where data points for all materials studied line up well in a double logarithmic plot, following the function

$$S\left(N_{Grains}\right) = 0.49 \cdot N_{Grains}^{-0.71}. \quad (1)$$

Note that in this fit S equals 0.49 for $N_{Grains} = 1$, which is very close to the theoretical value of 0.5 for a completely stochastic system of two distinct states of equal probability. The clear correlation observed between the stochasticity of crystallization observed in the PTE diagrams and the nucleation rate indicates that both quantities are closely interwoven, i.e., that one can be derived from the other. To rephrase this statement, if EBSD shows a low/high number of grains the crystallization will be of a stochastic/deterministic nature and vice versa.

To simulate crystallization under laser illuminations a multiphysics analysis has been performed. Here electromagnetic, heat transfer and phase transition simulations have been self-consistently coupled.[39] A change in the optical and thermal properties of the PCM has been taken into account. A phase field model was utilized to simulate the phase transition. The examples of $Ge_2Sb_2Te_5$ (Figure 5b) and GeTe (Figure 5c) reproduce the temporal evolution of crystallization experimentally. The two simulation runs for GeTe show a larger deviation from each other, while the two simulation runs for $Ge_2Sb_2Te_5$ practically coincide. This difference in behavior can be ascribed to the considerably low nucleation rate of GeTe compared to $Ge_2Sb_2Te_5$, i.e., the development of much fewer nuclei in GeTe compared to $Ge_2Sb_2Te_5$, in perfect agreement with the EBSD measurements. So far, it has been shown that the speed of nucleation governs the stochasticity and speed of the crystallization process. To further quantify this relation, the nucleation rate and the growth rate have to be determined.

4. Slow-Nucleation Materials

In the reflectance change data depicted in Figure 3c–e, the majority of pulses either create no major reflectance change or a well-defined, rather pronounced reflectance change. Please note that a minor reflectance change is observed even without crystallization, likely due to structural relaxation effects. A pronounced reflectance change is only observed if the material has been crystallized in the laser-illuminated region. This requires at least one nucleation event within this region. Since nucleation is a stochastic process, it can be described by a probability distribution for the first nucleus $P_N(t)$. 40 measurements were thus performed

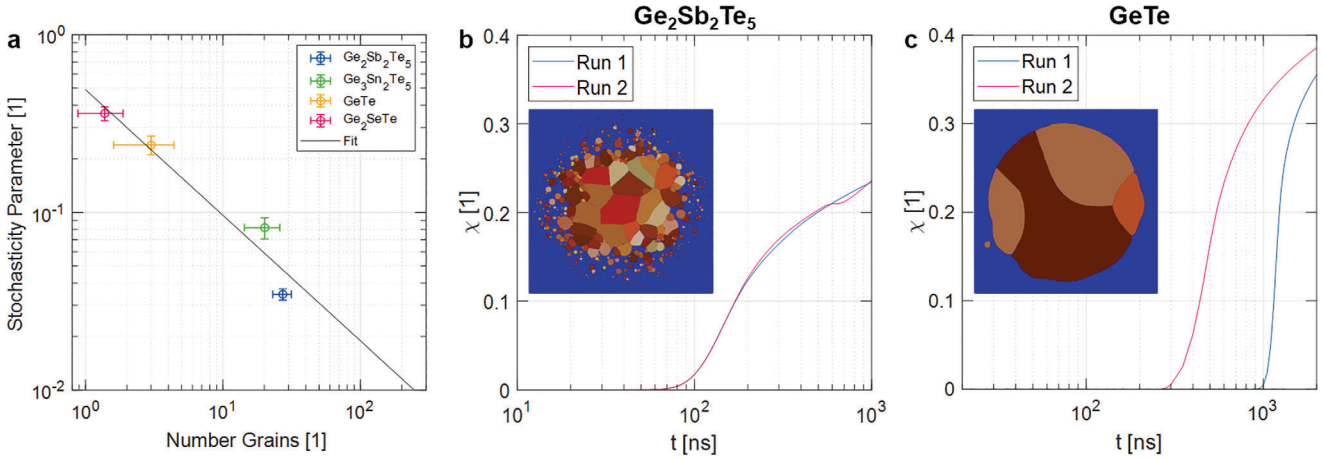

Figure 5. Stochasticity of crystallization S versus the number of grains N_{Grains} observed in EBSD measurements after the crystallization pulse a). All materials examined show a clear trend of decreasing stochasticity with an increasing number of grains formed in the illuminated region, as illustrated by a linear fit in the double logarithmic plot. Different runs of multiphysics simulation of the crystallization process of $Ge_2Sb_2Te_5$ b) show a nearly identical macroscopic development of the crystal volume fraction χ. The inlet shows the simulated grain structure. The high number of nuclei agrees very well with the EBSD measurements. For the two runs of GeTe c) a significantly different evolution of crystallization is found, due to the stochastics of the nucleation of a small number of clusters. Again, the simulation closely matches the EBSD measurement. The associated time-dependent grain structure is given in (Figures S8 and S9, Supporting Information).

for each pulse length to determine $P_N(t)$. The increase of P_N with time t depends upon the average nucleation rate $J(t)$ multiplied by the probability that a region can still crystallize $(1 - P_N(t))$, which leads to the equation

$$\frac{\partial P_N}{\partial t} = J(t)\left(1 - P_N(t)\right) \tag{2}$$

This differential equation is solved by an exponential function,

$$P_N(t) = 1 - \exp\left(-\int_0^t dt' J(t')\right) \tag{3}$$

which only depends on the nucleation rate. The Gompertz function gives a sufficient fit for the three systems GeTe, AIST, and Ge_2SeTe. It can be given in the form

$$P_N(t) = \exp\left(-\exp\left(a\left(b - t\right)\right)\right) \tag{4}$$

where a and b are fit parameters. With this finding a constant nucleation rate can be excluded, since the majority of observed nucleation takes place in the transient regime. From the probability distribution, the expected nucleation time t_N can be calculated. Further discussion on the time-dependent nucleation rate can be found in the supplementary information (Figures S12–S14, Supporting Information).

Significant crystal growth requires a multitude of single-atom attachment events to the crystalline cluster. Because of the large number of events that are stochastic in themselves, the entirety of growth can be considered not to be stochastic, but deterministic. Therefore, under identical conditions, all growth processes need the same time t_G to proceed after nucleation has occurred. A growth process can only be detected if the reflectance is in between that of the amorphous and fully crystallized state. The nucleation event has to occur before the end of the pulse but not so long before that the growth would already have ended, leading to the equation for the probability of a growth event

$$P_G(t) = P_N(t) - P_N\left(t - t_G\right) \tag{5}$$

where t_G is the growth time. The expected number of observed growth events for every pulse length can then be calculated as the product of P_G for the respective pulse length and the number of measurements, i.e., 1600, as presented in Figures S12d,S13d, and S14d (Supporting Information). The number of measurements was increased to compensate for the generally low number of observed growth events of the slow-nucleation materials compared to the number of nucleation events. The pulse length-dependent number of observed growth events agrees well with the model described, even though it only has a single free parameter (t_G). This validates the assumption of a constant growth time, which is determined to be 3.6×10^2 ns for GeTe, 3.9×10^2 ns for AIST, and 1.1×10^3 ns for Ge_2SeTe.

5. Fast-Nucleation Materials

In the case of the fast-nucleation systems $Ge_2Sb_2Te_5$ and $Ge_3Sn_2Te_5$, the reflectance change switches continuously from the amorphous to the crystalline level, as shown in Figure 3a,b. Hence, there is no possibility to observe independent nucleation events as seen for the slow-nucleation systems. This prohibits a comparably precise examination of the time dependence of nucleation. Nevertheless, an approximation of the time to form the first nucleus t_N as well as the growth time t_G can be obtained. This enables a comparison of all five-phase change materials studied. To this end, an upper boundary for the time required to form the first nucleus can be identified as the length of the onset pulse length t_{ON} for which the reflectance change in Figure 3a,b first shows clear signs of crystallization, i.e., a distinct increase above

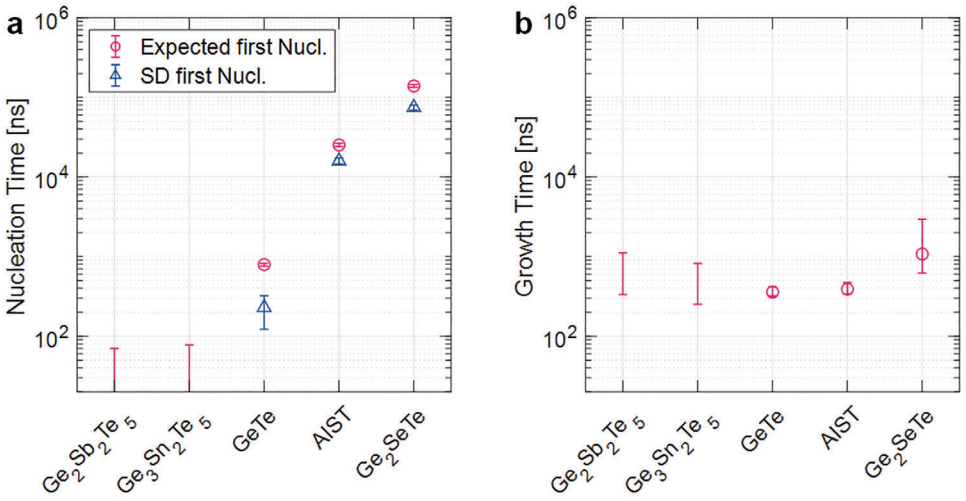

Figure 6. a) Time required for the first nucleation event for different phase change materials. A significant stoichiometry dependence is observed. For slow-nucleation materials, the standard deviation for the probability distribution is given as well. All data points are given with uncertainties of determinability for the used method. These are very small for slow-nucleation materials. Further information on this can be found in (Figures S11–S14, Supporting Information). b) Growth time for all materials, showing only a marginal dependence on stoichiometry.

the reflectance of the amorphous state (see Figure S15, Supporting Information for details).

Crystal growth happens from this onset t_{ON} until the end of crystallization t_C, which also can be approximated from Figure 3a b. To determine the crystal growth rate, we have to consider the number of grains that contribute to the crystallization process. For the slow-nucleation materials, this is only a single grain. However, for $Ge_2Sb_2Te_5$ and $Ge_3Sn_2Te_5$, several grains contribute. Hence, the growth time has to be rescaled by the number of grains in the region illuminated. For an estimate of the radial velocity this leads to a correction factor by the square root of the number of grains N_{Grains} leading to the equation

$$t_G = \left(t_C - t_{ON}\right) \cdot \sqrt{N_{Grains}} \tag{6}$$

The results, for both t_N and t_G, are shown in the next section together with the slow-nucleation materials.

6. Comparing the Crystallization Kinetics for Different Phase Change Materials

The main results of the last two sections are gathered in **Figure 6**, where the time needed for the first nucleation event as well as the growth time is depicted for all materials studied. This figure shows that the time for the first nucleation changes drastically with stoichiometry and increases by over 3 orders of magnitude. On the contrary, the growth time hardly changes with stoichiometry. This shows that the maximum crystallization speed is governed by the nucleation rate and not the growth rate. Hence fast-nucleation materials crystallize much faster than slow-nucleation materials. Yet, if nucleation were not needed to recrystallize a certain region of material, i.e., crystalline nuclei with sufficient size were already available, the growth process transforming the material into a fully crystalline region would not show a pronounced stoichiometry dependence.

7. Conclusion and Comparison with Previous Work

Understanding the mechanism of fast crystallization in phase change materials has motivated a plethora of different investigations. Yet, unraveling the contribution of nucleation and growth on these short time and length scales is very challenging. Therefore, in the past, studies were often performed on longer time scales where only spatial resolution was crucial. A characteristic example of such studies has been published by Kalb et al., who already found that nucleation behavior differs more drastically between $Ge_2Sb_2Te_5$ and AIST as compared to growth velocity.[59] They employed atomic force microscopy studies of thermally crystallized regions on time scales of seconds to hours and unraveled significant differences in nucleation rate. This observation has been attributed to lower interfacial energy between the amorphous and crystalline phases and a lower reduced glass transition temperature for $Ge_2Sb_2Te_5$.[60] It would be very tempting to extend such an investigation to the other compounds studied here, i.e., GeTe, Ge_2SeTe, and $Ge_3Sn_2Te_5$. Yet, such experiments are very tedious and would constitute a study in its own right. This is beyond the scope of the present investigation. To obtain data at a much higher temperature, where crystallization can proceed on a nanosecond time scale relevant to device operation, fast pulse experiments are required. The need to unravel nucleation and growth has motivated ingenious studies by Coombs et al.[61,62] By applying short laser pulses, they could distinguish nucleation from the start of crystallization in as-deposited samples and crystal growth from the complete erasure time of amorphous spots in a crystalline matrix. These studies have determined the crystal growth velocity to speeds of several m s^{-1} up to several 10 m s^{-1}, in line with the required growth time of $\approx 3 \times 10^2$ ns for a region of ≈ 1 µm. Their investigations on the complete erasure time are of high importance for the possible implementation of very small switching cells like for phase change random-access memories, since these would not depend on nucleation due to growth from the surrounding

crystalline material. However, larger cells as anticipated in photonic applications will have to rely on nucleation and subsequent growth, which is covered in the current study.

In addition, it is highly desirable to directly observe the different grains that have formed upon crystallization. In the present study, the use of EBSD measurements enables the identification of different grains' sizes and orientations. The combination of short laser pulses and EBSD enables the determination of the underlying crystallization mechanisms that take place on nanosecond time scales, producing crystalline grains of just 10 to 100 nm. These experiments unambiguously reveal that the nucleation rate governs both the crystallization speed as well as the origin of the stochasticity of crystallization for phase change materials. In particular, we could identify $Ge_2Sb_2Te_5$ and $Ge_3Sn_2Te_5$ as fast-nucleation materials, while GeTe, AIST, and Ge_2SeTe are slow-nucleation materials. For the commonly used $Ge_2Sb_2Te_5$, GeTe, and AIST, this classification is in line with previous studies.[63,64]

There are two further directions of study that are motivated by the present findings. First of all, it would be interesting to significantly increase the database for fast crystallization in phase change materials by exploring a significantly larger number of materials. This would enable a validation of the hypothesis that there is a much more pronounced stoichiometry dependence for the nucleation rate than the maximum growth rate. Recently it has already been shown that the crystallization speed is closely related to the stoichiometry of phase change materials, relating this speed in particular to the bonding of the crystalline phases.[42] As previously mentioned, the crystalline phase change materials studied here all employ metavalent bonding. It would be interesting to extend the present investigation to a much wider range of these metavalent solids. Furthermore, it would be interesting to understand why the maximum growth speed seems to be rather independent of material stoichiometry.

8. Experimental Section

Sample Layout and Preparation: To investigate the effects of nucleation and growth separately this study deals with completely amorphous sputtered samples. This way it can be made sure that crystallization initially always requires nucleation which might not be the case for recrystallizing melt-quenched spots in a crystalline matrix. In this case, there might also be crystallization processes that only consist of growth from the remaining crystalline grains at the border of the amorphized region.

$Ge_2Sb_2Te_5$, GeTe, and AIST are sputtered from stoichiometric targets, while $Ge_3Sn_2Te_5$ and Ge_2SeTe were co-sputtered. To keep the temperature difference in the sample as small as possible the PCM layer in the samples was kept thin at 30 nm and a heat barrier of 10 nm of $(ZnS)_4(SiO_2)$ was added between the PCM and Silicon substrate. A capping layer of 100 nm of $(ZnS)_4(SiO_2)$ was added on top of the PCM to prevent it from oxidation and evaporation of portions of the PCM during heating.

Optically Induced Crystallization Experiments: A pump-probe setup was used to crystallize the sample. The pump laser had a wavelength of 658 nm and was triggered by an arbitrary wave generator with pulses down to 10 ns. The continuous probe laser had a wavelength of 639 nm and was driven at a laser power of 50 µW. Its power was measured in the incoming as well as the outgoing beam before and after the pulse to determine the reflectance change. To ensure an ideal alignment of the lasers they are both coupled into a mono-mode fiber. The lasers were focused onto the sample to a spot size of 2.3 µm ($1/e^2$) in diameter.

Electron Backscatter Diffraction: The top layer $(ZnS)_4(SiO_2)$ is removed prior to the EBSD measurements by submerging the sample in 1% Hydrofluoric acid for 2 min. After this, the samples were loaded in a Dual Beam FIB-SEM Helios NanoLab from FEI/Thermo Fischer Scientific, with an attached EBSD detector (AMETEK, NJ, USA). The SEM was operated with an acceleration voltage of 20 keV and a beam current of 1.6 nA, with a chamber pressure of $\approx 10^{-6}$ mbar. The sample tilt and working distance were set to 70° and 13 mm, respectively. With these parameters, the EBSD lateral resolution was ≈30 nm. In the images shown in the paper, the inverse pole figure of the pole perpendicular to the sample surface is shown. To distinguish between the amorphous matrix and the crystallized spot, the image's brightness values were dependent on the image quality, i.e., the similarity between neighboring frames. Without any long-range order, the amorphous matrix is shown as black, while the crystallized regions are visible. An example of the separate Image quality and Inverse pole figure maps is shown in Figure S1 (Supporting Information).

Multiphysics Simulations: As a comparison to the experimental results, a self-consistent multiphysics simulation was performed. The multiphysics model consists of electromagnetic and thermal simulations conducted using the commercial software CST-Studio Suite[65] in combination with custom phase field crystallization simulations as described in.[39] In the electromagnetic simulation, a Gaussian beam with a power of 39 mW at a wavelength of 658 nm and a beam radius of 1220 nm was used as a field source. The electromagnetic losses in the layer stack were used as a heat source for the thermal simulation. The resulting temperature was then used in the crystallization simulation. A domain of 1500 nm x 1500 nm x 30 nm divided into voxels of 1 nm x 1 nm x 1 nm was simulated. The updated crystalline distribution was then used in the next time step to adjust the material properties of the electromagnetic and thermal simulations. The time step of the simulations is varied depending on the rate of temperature change in the PCM layer ranging from 1 to 50 ns.

Supporting Information

Supporting Information is available from the Wiley Online Library or from the author.

Acknowledgements

This work was supported in part by the Deutsche Forschungsgemeinschaft (SFB 917) and in part by the Federal Ministry of Education and Research (BMBF, Germany) in the project NEUROTEC II (16ME0398K). P.L. acknowledges support from NSF-DMR grant 2067890. D.N.C. acknowledges partial support by the Deutsche Forschungsgemeinschaft through a Heisenberg Fellowship (CH 407/13-1) and the project (CH 407/15-1). The authors also acknowledge the work of Christoph Persch and Oliver Krause who helped prepare samples, Yuan Yu for giving advice on performing EBSD experiments and Julian Pries for giving advice on performing and evaluating the SAED experiments. Additionally, the authors acknowledge Christoph Persch for helping to conceptualize the project at an early stage.

Open access funding enabled and organized by Projekt DEAL.

Conflict of Interest

The authors declare no conflict of interest.

Author Contributions

M.J.M., C.M., and M.W. conceptualized the project and designed the experiments; M.J.M., C.M., C.S., and J.W. prepared samples; M.J.M. conducted the crystallization experiments; P.K., M.R., and R.P. performed

EBSD experiments; S.M. and D.N.C. conducted the multiphysics simulations; C.S. performed the SAED experiments; P.K., S.M., C.S., D.N.C., and P.L. provided comments for the manuscript with support from all coauthors; M.J.M. and M.W. wrote the paper. All authors have approved the final version of the manuscript.

Data Availability Statement

The data that support the findings of this study are available from the corresponding author upon reasonable request.

Keywords

crystal growth, crystallization kinetics, electron backscatter diffraction, materials design, metavalent bonding, nucleation, phase change materials

Received: February 27, 2024
Revised: April 22, 2024
Published online: May 11, 2024

[1] T. Döhring, R. Jedamzik, A. Thomas, P. Hartmann, in Advanced Optical and Mechanical Technologies in Telescopes and Instrumentation, Marseille, France **2008**, 1154.
[2] J. Orava, A. á. Greer, B. Gholipour, D. Hewak, C. Smith, *Nat. Mater.* **2012**, *11*, 279.
[3] M. Salinga, E. Carria, A. Kaldenbach, M. Bornhöfft, J. Benke, J. Mayer, M. Wuttig, *Nat. Commun.* **2013**, *4*, 2371.
[4] W. Zhang, R. Mazzarello, M. Wuttig, E. Ma, *Nat. Rev. Mater.* **2019**, *4*, 150.
[5] G. Johari, A. Hallbrucker, E. Mayer, *Nature* **1987**, *330*, 552.
[6] V. Velikov, S. Borick, C. Angell, *Science* **2001**, *294*, 2335.
[7] A. L. Greer, K. F. Kelton, *J. Am. Ceram. Soc.* **1991**, *74*, 1015.
[8] M. Xu, X. Mai, J. Lin, W. Zhang, Y. Li, Y. He, H. Tong, X. Hou, P. Zhou, X. Miao, *Adv. Funct. Mater.* **2020**, *30*, 2003419.
[9] D. Loke, T. Lee, W. Wang, L. Shi, R. Zhao, Y. Yeo, T. Chong, S. Elliott, *Science* **2012**, *336*, 1566.
[10] M. L.e Gallo, T. Tuma, F. Zipoli, A. Sebastian, E. Eleftheriou, presented at 2016 46th European Solid-State Device Research Conference (ESSDERC), Lausanne, Switzerland September **2016**.
[11] J. Pries, S. Wei, M. Wuttig, P. Lucas, *Adv. Mater.* **2019**, *31*, 1900784.
[12] G. Bruns, P. Merkelbach, C. Schlockermann, M. Salinga, M. Wuttig, T. Happ, J. Philipp, M. Kund, *Appl. Phys. Lett.* **2009**, *95*, 043108.
[13] A. Sebastian, M. Le Gallo, D. Krebs, *Nat. Commun.* **2014**, *5*, 4314.
[14] J. Torrent-Burgués, *J. Cryst. Growth* **1994**, *140*, 107.
[15] K. Kelton, A. Greer, *Phys. Rev. B* **1988**, *38*, 10089.
[16] K. Kelton, A. L. Greer, C. Thompson, *J. Chem. Phys.* **1983**, *79*, 6261.
[17] M. Volmer, A. Weber, *Zeitschrift für physikalische Chemie* **1926**, *119*, 277.
[18] R. Becker, W. Döring, *Ann. Phys.* **1935**, *416*, 719.
[19] D. Turnbull, J. C. Fisher, *J. Chem. Phys.* **1949**, *17*, 71.
[20] R. C. Miller, R. J. Anderson, J. Kassner Jr, D. E. Hagen, *J. Chem. Phys.* **1983**, *78*, 3204.
[21] C. Brandel, J. H. ter Horst, *Faraday Discuss.* **2015**, *179*, 199.
[22] F. Rao, K. Ding, Y. Zhou, Y. Zheng, M. Xia, S. Lv, Z. Song, S. Feng, I. Ronneberger, R. Mazzarello, *Science* **2017**, *358*, 1423.
[23] M. A. Caldwell, S. Raoux, R. Y. Wang, H.-S. P. Wong, D. J. Milliron, *J. Mater. Chem.* **2010**, *20*, 1285.
[24] Y. Zhou, W. Zhang, E. Ma, V. L. Deringer, *Nat. Electron.* **2023**, *6*, 746.
[25] J. Hegedus, S. R. Elliott, *Nat. Mater.* **2008**, *7*, 399.
[26] G. C. Sosso, G. Miceli, S. Caravati, F. Giberti, J. r. Behler, M. Bernasconi, *J. Phys. Chem. Lett.* **2013**, *4*, 4241.
[27] Y. Xu, Y. Zhou, X. D. Wang, W. Zhang, E. Ma, V. L. Deringer, R. Mazzarello, *Adv. Mater.* **2022**, *34*, 2109139.
[28] Y. Zhou, W. Zhang, E. Ma, V. L. Deringer, arXiv preprint arXiv:2207.14228 **2022**.
[29] J.-Y. Raty, C. Bichara, C.-F. Schön, C. Gatti, M. Wuttig, *Proc. Natl. Acad. Sci. USA* **2024**, *121*, 2316498121.
[30] B. J. Kooi, M. Wuttig, *Adv. Mater.* **2020**, *32*, 1908302.
[31] M. Wuttig, C. F. Schön, J. Lötfering, P. Golub, C. Gatti, J. Y. Raty, *Adv. Mater.* **2023**, *35*, 2208485.
[32] M. Wuttig, V. L. Deringer, X. Gonze, C. Bichara, J. Y. Raty, *Adv. Mater.* **2018**, *30*, 1803777.
[33] C.-F. Schön, S. van Bergerem, C. Mattes, A. Yadav, M. Grohe, L. Kobbelt, M. Wuttig, *Sci. Adv.* **2022**, *8*, eade0828.
[34] M. Zhu, O. Cojocaru-Miredin, A. M. Mio, J. Keutgen, M. Kupers, Y. Yu, J. Y. Cho, R. Dronskowski, M. Wuttig, *Adv. Mater.* **2018**, *30*, 1706735.
[35] J. Y. Raty, M. Schumacher, P. Golub, V. L. Deringer, C. Gatti, M. Wuttig, *Adv. Mater.* **2019**, *31*, 1806280.
[36] Y. Cheng, O. Cojocaru-Mirédin, J. Keutgen, Y. Yu, M. Küpers, M. Schumacher, P. Golub, J. Y. Raty, R. Dronskowski, M. Wuttig, *Adv. Mater.* **2019**, *31*, 1904316.
[37] L. Guarneri, S. Jakobs, A. von Hoegen, S. Maier, M. Xu, M. Zhu, S. Wahl, C. Teichrib, Y. Zhou, O. Cojocaru-Miredin, M. Raghuwanshi, C. F. Schon, M. Drogeler, C. Stampfer, R. Lobo, A. Piarristeguy, A. Pradel, J. Y. Raty, M. Wuttig, *Adv. Mater.* **2021**, *33*, 2102356.
[38] M. Avrami, *J. Chem. Phys.* **1940**, *8*, 212.
[39] S. Meyer, Z. Y. Tan, D. N. Chigrin, *Nanophotonics* **2020**, *9*, 675.
[40] F. Humphreys, *J. Mater. Sci.* **2001**, *36*, 3833.
[41] Y. Wang, P. Chao, S. Moniri, J. Gao, T. Volkenandt, V. De Andrade, A. J. Shahani, *Mater. Charact.* **2020**, *170*, 110685.
[42] C. Persch, M. J. Müller, A. Yadav, J. Pries, N. Honné, P. Kerres, S. Wei, H. Tanaka, P. Fantini, E. Varesi, *Nat. Commun.* **2021**, *12*, 4978.
[43] K. Kato, M. Kuwahara, H. Kawashima, T. Tsuruoka, H. Tsuda, *Appl. Phys. Express* **2017**, *10*, 072201.
[44] Y. Zhang, C. Fowler, J. Liang, B. Azhar, M. Y. Shalaginov, S. Deckoff-Jones, S. An, J. B. Chou, C. M. Roberts, V. Liberman, *Nat. Nanotechnol.* **2021**, *16*, 661.
[45] S. Raoux, H.-Y. Cheng, M. Caldwell, H.-S. Wong, *Appl. Phys. Lett.* **2009**, *95*, 071910.
[46] C. Stenz, J. Pries, T. W. Surta, M. W. Gaultois, M. Wuttig, *Adv. Sci.* **2023**, 2304323.
[47] X. Sun, E. Thelander, J. W. Gerlach, U. Decker, B. Rauschenbach, *J. Phys. D: Appl. Phys.* **2015**, *48*, 295304.
[48] J. Park, M. R. Kim, W. S. Choi, H. Seo, C. Yeon, *Jpn. J. Appl. Phys.* **1999**, *38*, 4775.
[49] F. Tabatabaei, G. Boussinot, R. Spatschek, E. A. Brener, M. Apel, *J. Appl. Phys.* **2017**, *122*, 045108.
[50] Y. Chen, G. Wang, L. Song, X. Shen, J. Wang, J. Huo, R. Wang, T. Xu, S. Dai, Q. Nie, *Cryst. Growth Des.* **2017**, *17*, 3687.
[51] T. Nirschl, J. Philipp, T. Happ, G. W. Burr, B. Rajendran, M.-H. Lee, A. Schrott, M. Yang, M. Breitwisch, C.-F. Chen, presented at 2007 IEEE Int. Electron Devices Meeting, IEEE, Washington, DC, USA December **2007**.
[52] I. Bolotov, V. Y. Kolosov, A. Kozhyn, *physica status solidi* **1982**, *72*, 645.
[53] B. Kooi, W. Groot, J. T. M. De Hosson, *J. Appl. Phys.* **2004**, *95*, 924.
[54] Y. Cao, H. Di, J. Zhang, J. Zhang, T. Ma, R. Misra, *Mater. Sci. Eng.* **2013**, *585*, 71.
[55] V. Y. Kolosov, A. Thölen, *Acta Mater.* **2000**, *48*, 1829.
[56] B. Kooi, J. T. M. De Hosson, *J. Appl. Phys.* **2004**, *95*, 4714.
[57] J. Kalb, F. Spaepen, M. Wuttig, *J. Appl. Phys.* **2003**, *93*, 2389.
[58] S. Jiang, J. H. ter Horst, *Cryst. Growth Des.* **2011**, *11*, 256.

[59] J. Kalb, F. Spaepen, M. Wuttig, *Appl. Phys. Lett.* **2004**, *84*, 5240.
[60] J. Kalb, F. Spaepen, M. Wuttig, *J. Appl. Phys.* **2005**, *98*, 054910.
[61] J. Coombs, A. Jongenelis, W. van Es-Spiekman, B. Jacobs, *J. Appl. Phys.* **1995**, *78*, 4906.
[62] J. Coombs, A. Jongenelis, W. van Es-Spiekman, B. Jacobs, *J. Appl. Phys.* **1995**, *78*, 4918.
[63] K. Ohara, L. Temleitner, K. Sugimoto, S. Kohara, T. Matsunaga, L. Pusztai, M. Itou, H. Ohsumi, R. Kojima, N. Yamada, *Adv. Funct. Mater.* **2012**, *22*, 2251.
[64] N. Yamada, E. Ohno, N. Akahira, K. Nishiuchi, K. Nagata, M. Takao, *Jpn. J. Appl. Phys.* **1987**, *26*, 61.
[65] CST-Studio Suite, https://www.3ds.com/products-services/simulia/products/cst-studio-suite (accessed: January 2024).